

Single-mode versus multimode behavior in silicon photonic crystal waveguides measured by attenuated total reflectance

M. Galli

Istituto Nazionale per la Fisica della Materia and Dipartimento di Fisica "A. Volta," Università di Pavia, via Bassi 6, 27100 Pavia, Italy

D. Bajoni,* M. Patrini, G. Guizzetti, D. Gerace, and L. C. Andreani
Dipartimento di Fisica "A. Volta," Università di Pavia, via Bassi 6, 27100 Pavia, Italy

M. Belotti

Dipartimento di Fisica "A. Volta," Università di Pavia, via Bassi 6, 27100 Pavia, Italy
and Laboratoire de Photonique et de Nanostructures, CNRS, Route de Nozay, 91460 Marcoussis, France

Y. Chen

Département de Chimie, Ecole Normale Supérieure, 24 Rue Lhomond, 75231 Paris Cedex 05, France
and Laboratoire de Photonique et de Nanostructures, CNRS, Route de Nozay, 91460 Marcoussis, France

(Received 22 March 2005; revised manuscript received 12 July 2005; published 15 September 2005)

Linear photonic crystal waveguides with different channel widths realized in silicon membranes are investigated by means of attenuated-total-reflectance (ATR) measurements. The dispersion of line-defect modes with both parities with respect to a vertical plane bisecting the waveguide channel is determined, thereby allowing one to distinguish between multimode and single-mode behavior. The presence of a single-mode frequency window in the guided-mode region below the light line is established not only for standard W1 waveguides with channel width $w_0 = \sqrt{3}a$ (i.e., a missing row of holes in the triangular lattice with lattice constant a), but also for W1.5 waveguides where the channel width is increased to $w = 1.5w_0$. The results agree with theoretical predictions and might be important for the realization of linear photonic crystal waveguides with single-mode behavior and ultralow propagation losses.

DOI: [10.1103/PhysRevB.72.125322](https://doi.org/10.1103/PhysRevB.72.125322)

PACS number(s): 42.70.Qs, 42.82.Et, 78.20.Bh, 78.40.Fy

I. INTRODUCTION

Linear photonic crystal (PhC) waveguides for the control of light propagation can be realized either in fully three-dimensional (3D) structures with a complete band gap,¹ or in quasi-3D systems like PhC slabs.^{2,3} In the latter structures, a two-dimensional (2D) photonic lattice is defined in a planar waveguide and confinement of light in the third dimension is obtained by means of total internal reflection within the slab. Introducing defects in the periodic array of the 2D pattern enables to create propagating defect modes within the photonic band gap. For high-index PhC slabs like the self-standing membrane or air bridge, truly guided-wave propagation with very low losses can be obtained for modes lying below the air light line in the k - ω plane.⁴⁻⁸ In this region, propagation losses are purely extrinsic as they are determined only by roughness, or disorder-induced scattering. The most thoroughly studied system is the so-called W1 waveguide, consisting of a missing row of holes in the Γ - K symmetry direction of the triangular lattice (see Fig. 1). Very low propagation losses have been demonstrated for W1 waveguides defined in silicon⁹⁻¹¹ and GaAs¹² membranes. Recent theoretical predictions based on a model for disorder-induced out-of-plane scattering¹³ indicate that the losses could be further reduced by increasing the channel width of the linear waveguide.^{14,15} Furthermore, it is also important to have a high group velocity region in the guided-mode dis-

persion in order to reduce propagation losses.^{16,17}

In addition to the goal of achieving low propagation losses, a very important requirement is that of having single-mode behavior in a given frequency region. Recently, scattering of light into modes with different symmetries has been demonstrated in straight line defects.¹⁸ Indeed, when bent waveguides or more complex 2D interconnections are realized, the existence of two or several modes at the same frequency can give rise to modal coupling, thus limiting the device performance. Increasing the channel width of a linear waveguide tends to give multimode behavior, as several modes may be supported by the wider channel structure. It is therefore quite important to establish the best parameters for

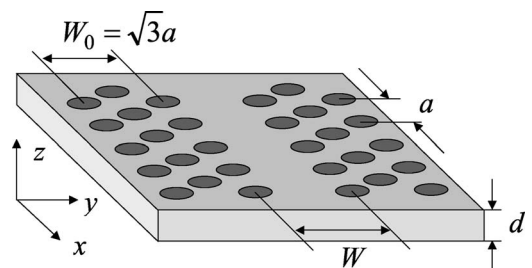


FIG. 1. Schematic structure of a linear waveguide along the Γ - K direction of the triangular lattice, defined in a self-standing membrane of thickness d . For a W1.0 waveguide, the channel width w equals $w_0 = \sqrt{3}a$, where a is the lattice constant.

linear PhC waveguides, which yield at the same time single-mode behavior in a high group velocity region and the lowest possible propagation losses. From a fundamental point of view, it is also important to demonstrate *experimentally* that a structure realized according to the theoretical design does indeed have the required characteristics.

In this work we show that a convenient region of single-mode behavior exists in linear waveguides with increased channel width. We determine the dispersion of line-defect modes for PhC waveguides in silicon membranes by means of variable-angle attenuated-total-reflectance (ATR) measurements from the slab surface. This technique was recently shown¹⁹ to yield the dispersion of photonic modes below the light line in silicon-on-insulator (SOI) PhC slabs. For a W1.5 waveguide (i.e., when the channel width is increased to $w = 1.5w_0$; see Fig. 1) we establish the presence of a high group velocity frequency region below the light line in which only the fundamental defect mode exists. These results are in agreement with theoretical predictions for the dispersion of defect modes in increased-width waveguides. In particular, it is shown here that ATR measurements for different orientations of the sample allow probing the parity symmetry of the waveguide modes with respect to a vertical plane bisecting the waveguide channel, thus allowing a direct determination of the single-mode propagation window. Furthermore, the group index of the defect modes is determined and is shown to reach very high values in the region of flat dispersion.

Experimental studies of increased-width waveguides in high-index contrast PhC slabs were previously performed for SOI systems,²⁰ where the phase-space region below the light line is limited because of the presence of the lower SiO₂ cladding. Indeed, a better tailoring of the defect-mode dispersion and a reduction of the losses in SOI PhC slabs is obtained by using *reduced-width* waveguides.^{11,16,20} The defect mode dispersion of reduced-width PhC waveguides has been measured in silicon air bridges by using the Fabry-Pérot interference technique on samples of definite lengths.²¹ For self-standing high-index membranes, experimental studies of waveguides with increased channel width have not been performed yet. Increased-width waveguides are commonly studied in low-index contrast PhC slabs based on GaAs^{22,23} or InP,²⁴ where the physical behavior is quite different from that discussed here since all modes lie above the light line of the cladding material (therefore being subject to intrinsic diffraction losses) and the mode dispersion is close to that of the corresponding 2D photonic structure.

The paper is organized as follows. In Sec. II we present theoretical calculations of the defect-mode dispersion in increased-width waveguides and discuss the selection rules for excitation of the modes in surface-reflectance experiments. In Sec. III we show and discuss the experimental results for ATR spectra, defect-mode dispersion and group index. Section IV, finally, contains concluding remarks. We point out that this work extends the one previously published by us¹⁹ in several respects: (i) the present experiments are performed on *single* line-defect waveguides in *self-standing Si membranes* (instead of periodically repeated defects in SOI slabs); (ii) the capability to measure the dispersion below the light line by ATR is greatly enhanced by the use of a silicon (instead of a ZnSe) prism; (iii) the focus here is a

systematic study of the defect-mode dispersion as a function of the PhC waveguide channel width.

II. THEORETICAL MODELING

The dispersion of line-defect modes in PhC slabs is calculated by means of the guided-mode expansion (GME) method introduced in Ref. 25. Briefly, the magnetic field is expanded in a finite basis set consisting of the guided modes of an effective homogeneous waveguide with an average dielectric constant in each layer. The second-order equation for the magnetic field becomes a linear eigenvalue problem containing the Fourier components of the inverse dielectric tensor, which is responsible for band folding and splittings. The method allows calculating the dispersion of photonic modes below and above the light line and also the radiative losses due to out-of-plane diffraction. Results concerning photonic band dispersion and intrinsic as well as extrinsic out-of-plane losses in PhC slabs with either 1D or 2D patterns in the slab plane have been published elsewhere.^{13,14,26–28} The accuracy of the GME method has been tested by comparisons with exact scattering matrix calculations²⁵ as well as with experimental measurements of photonic mode dispersion.^{19,29}

We consider here a triangular lattice of holes with lattice constant a , with a line-defect consisting of a missing row of holes in the $\Gamma-K$ direction, realized in a slab of thickness d with dielectric constant $\epsilon=12$ (see a schematic picture of the structure in Fig. 1). In Fig. 2 we present the calculated dispersion of line-defect modes for channel width increasing from $w=w_0 \equiv \sqrt{3}a$ (W1.0 waveguide) to $w=1.5w_0$ (W1.5 waveguide), assuming $d/a=0.575$ and hole radius $r/a=0.32$. Taking the origin of the z axis to be at the middle of the slab, specular reflection with respect to the (x,y) plane is a symmetry operation, which we denote by $\hat{\sigma}_{xy}$: we consider only modes with $\sigma_{xy}=+1$ (sometimes called TE-like modes), for which the triangular lattice has a band gap in all directions. Furthermore, defect modes are classified according to reflection symmetry with respect to the plane bisecting the channel, denoted as $\hat{\sigma}_{kz} \equiv \hat{\sigma}_{xz}$ operation: odd (even) modes with respect to vertical reflection symmetry have $\sigma_{kz}=-1$ ($\sigma_{kz}=+1$). Dark grey regions represent bulk modes of the PhC slab with a triangular lattice outside the band gap. In this case, the upper band edge is determined by the presence of a second-order mode cutoff for the effective slab waveguide, and is shown as a flat boundary in the figure.

It can be seen from Fig. 2 that, in the case of the W1.0 waveguide, a region of single-mode propagation below the light line occurs for the $\sigma_{kz}=-1$ mode at frequencies $\omega a/(2\pi c)$ between 0.268 and 0.281 (highlighted region in figure), as it is well known.^{7,16,21} For this case, the $\sigma_{kz}=-1$ defect mode is to a good approximation an index-guided mode, whose dispersion is close to that of a slab mode folded by the lattice periodicity. The single-mode region becomes narrower for the W1.1 waveguide and disappears almost completely for the W1.2 waveguide, due to the red shift of the gap-guided defect mode with symmetry $\sigma_{kz}=+1$. However, another region of single-mode propagation occurs on increasing the channel width beyond $w=1.3w_0$. For the W1.5 waveguide, single-mode propagation below the light line oc-

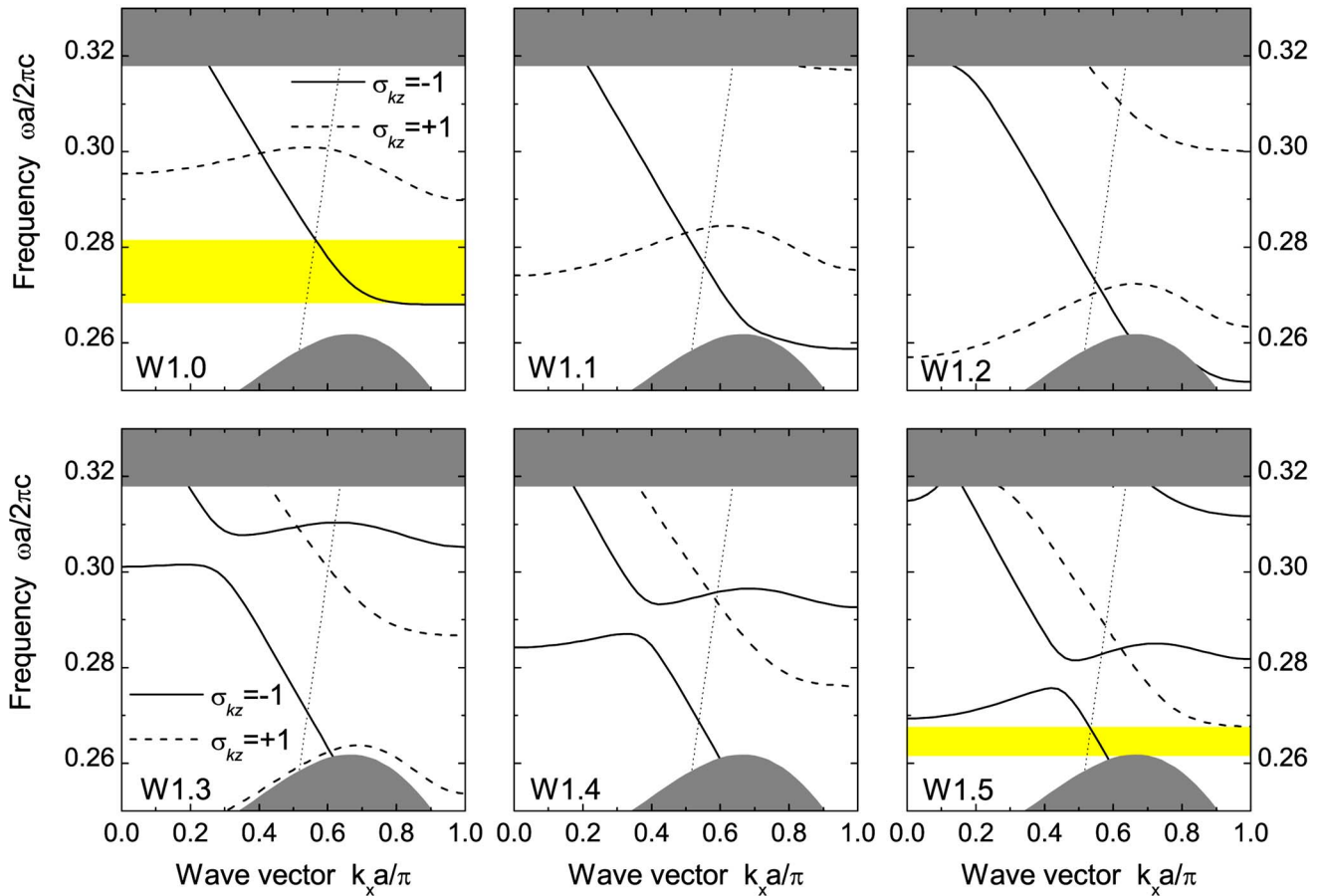


FIG. 2. (Color online) Dispersion of defect modes in linear waveguides with channel width increasing from $w=w_0$ (W1.0 waveguide, top left) to $w=1.5w_0$ (W1.5 waveguide, bottom right). Modes with $\sigma_{kz}=-1$ ($\sigma_{kz}=+1$) parity are represented by solid (dashed) lines. The dotted line represents the light dispersion in air. Parameters of calculation: dielectric constant $\epsilon=12$, slab thickness $d/a=0.575$, and hole radius $r/a=0.32$. The frequency regions outside the photonic gap of the triangular lattice are represented by dark gray areas. The frequency window of single-mode propagation is highlighted for the W1.0 and W1.5 structures.

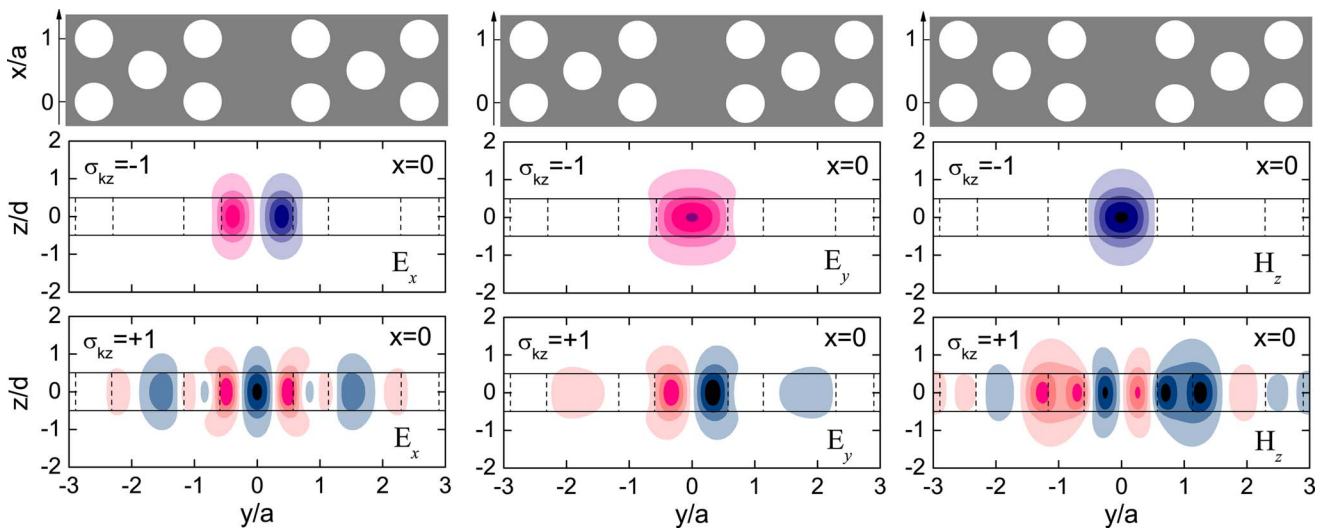


FIG. 3. (Color online) Profile of the field components E_x , E_y , and H_z in a W1.0 waveguide for the line-defect modes with $\sigma_{kz}=-1$ and $\sigma_{kz}=+1$, respectively. The field profiles are shown in the (y, z) plane at $x=0$. A scheme of the PhC waveguide in the (x, y) plane is also shown (top panels).

curs for dimensionless frequencies between 0.261 and 0.268 with group velocity close to c/n , where n is the refractive index of the core material. Single-mode propagation does not occur for waveguides with channel widths larger than $1.5w_0$ (not shown in Fig. 2). Therefore, the W1.5 waveguide is found to be the optimal structure that allows achieving single-mode propagation below the light line with a high group velocity and with the largest possible value for the channel width, implying very low propagation losses.¹⁴ Notice that even though the W1.0 waveguide has a larger single-mode frequency region than the W1.5 waveguide, the useful range where the mode group velocity has a weak dependence on frequency, leading to small propagation losses, is almost as wide as in the W1.5 waveguide.¹⁵

In Fig. 3 we show the spatial profiles of the field components E_x , E_y and H_z (which are the dominant ones for $\sigma_{xy} = +1$ or TE-like states) in the (y, z) plane for the $\sigma_{kz} = -1$ and $\sigma_{kz} = +1$ modes of a W1.0 waveguide. It is seen that E_y and H_z have qualitatively similar profiles, being spatially even (i.e., no nodes) with respect to the plane bisecting the channel for the $\sigma_{kz} = -1$ mode, whilst they are spatially odd (a node at $y=0$) for $\sigma_{kz} = +1$. On the other hand, the field profile of the E_x component is spatially odd for $\sigma_{kz} = -1$ and spatially even for $\sigma_{kz} = +1$. Considering that \mathbf{E} is a vector while \mathbf{H} is a pseudovector, it can be verified that the $\sigma_{kz} = -1$ mode is globally odd with respect to symmetry operation $\hat{\sigma}_{kz}$, while the $\sigma_{kz} = +1$ mode is globally even. Obviously, the global symmetry properties of an electromagnetic state are the same when derived from any of the electric- or magnetic-field components. These properties will be important for interpreting the optical experiments discussed in the next section.

III. EXPERIMENTAL RESULTS AND DISCUSSION

Free-standing silicon membranes patterned with a triangular lattice of air holes (lattice constant $a=0.4 \mu\text{m}$) and containing single line defects were fabricated by electron beam lithography and reactive ion etching techniques on Smart-Cut™ SOI wafers.³⁰ After lithographic definition and pattern transfer into the Si core, the underlying SiO_2 layer was removed by selective wet-etching in HF-based solution. The resulting $0.23\text{-}\mu\text{m}$ -thick free-standing Si membranes were $20 \mu\text{m}$ wide by $500 \mu\text{m}$ long, with a single line defect centered on the short side and extending along the full length of the membrane. Several samples with channel widths ranging from $w=w_0$ to $w=1.5w_0$ and nominal hole radius $r/a=0.32$ were prepared. In Figs. 4(a) and 4(b) close-up micrographs of the W1.0 and W1.5 samples are shown, respectively.

Angle-resolved ATR from the sample surface is measured in the spectral range $0.73\text{--}1.2 \text{ eV}$, at a spectral resolution of 0.5 meV , by means of a homemade microreflectometer coupled to a Fourier-transform spectrometer (Bruker IFS66s). The angle of incidence θ is varied in the range $20^\circ\text{--}60^\circ$ with an angular resolution of $\pm 0.5^\circ$ defined by the small aperture of the beam that is focused on the sample. Measurements are performed in transverse-electric (TE) polarization with respect to the plane of incidence, which is selected by means of a calcite Glan-Taylor polarizer.

The experimental geometry of ATR measurements is sketched in Fig. 5, where θ defines the incidence angle while

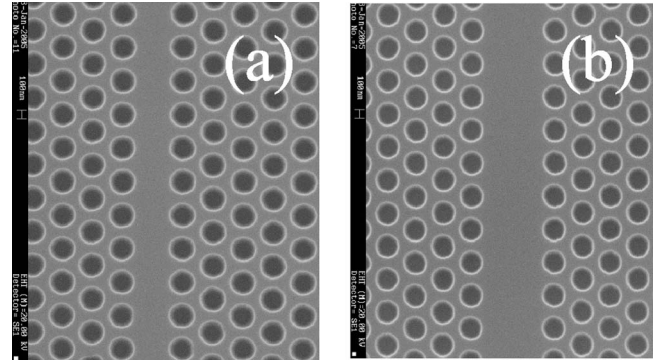


FIG. 4. Scanning electron micrographs of (a) W1.0 and (b) W1.5 samples, respectively. Lattice constant is $a=0.4 \mu\text{m}$ and membrane thickness is $0.23 \mu\text{m}$.

ϕ is the (azimuthal) rotation angle between the direction of the line defect and the plane of incidence. In order to excite the guided modes by ATR, a Si hemisphere acting as a prism is suspended over the membranes at a very small distance (typically $t \sim 0.2 \mu\text{m}$) by means of three piezoelectric actuators. These allow both a precise alignment between hemisphere and sample surfaces and a fine control of the separation distance t (as indicated in Fig. 5). In fact, due to the exponential decay of the evanescent field in the air layer between the hemisphere and the sample surface, both these adjustments are extremely critical in the measurement. Moreover, the coupling strength to the guided modes of the membranes is strongly influenced by the separation distance t , which thus determines the visibility of the ATR signal. Care has been taken in keeping the sample and prism surface as clean as possible, in order to achieve the small values for the separation distance needed in the experiments. We perform angle-resolved ATR measurements by focussing light through the Si hemisphere onto the membrane samples. An

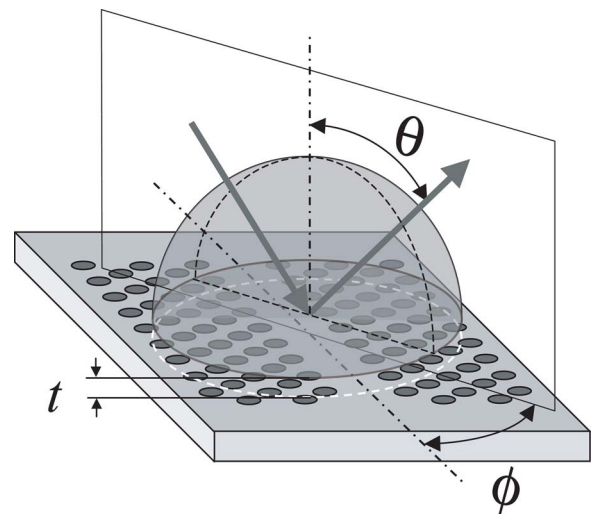


FIG. 5. (Color online) Schematic plot of the geometry used in ATR experiments. The silicon prism is kept at a distance t above the PhC; θ is the incidence angle while ϕ is the azimuthal angle between the direction of the line defect and the plane of incidence.

infrared vidicon camera is used to visualize the sample through the Si hemisphere, allowing a careful alignment of the line defect with respect to the plane of incidence. In order to avoid spurious contributions in the optical response, only the patterned region of the membranes containing a single line-defect was illuminated, thus resulting in a spot area of about $20 \mu\text{m} \times 50 \mu\text{m}$. We remark that Si hemisphere on the sample surface acts as a high-index solid immersion lens, thereby allowing to focalize the incident light well below the diffraction limit in air while keeping the very small numerical aperture needed for angular resolution.

The conceptual framework enabling the photonic mode dispersion to be mapped from ATR spectra at varying angles is similar to that employed to determine the dispersion of quasiguided modes in standard transmittance or reflectance experiments.^{31,32} In these techniques the resonant structure observed in the experimental spectra are plotted versus the wave vector component parallel to the sample surface (which is conserved), therefore yielding the photonic band dispersion above the light line. Under the experimental conditions of the present ATR measurements, the wave vector parallel to the sample surface is also conserved, and takes the value $k_{\parallel} = (n\omega/c)\sin\theta$ (modulo a reciprocal lattice vector), where n is the refractive index of the prism. Therefore, apart from achieving very small spot sizes, the choice of silicon as a high-index material for ATR measurements follows from the need to access high wave vector regions of the k - ω space for an efficient excitation of the defect modes. In fact, as already pointed out in Sec. II, the $\sigma_{k_z} = -1$ defect mode is characterized by a very steep dispersion, which is close to that of the unpatterned Si membrane. This means that even though the guided mode is folded back into the first Brillouin zone by lattice periodicity, its dominant wave vector component lies in the second Brillouin zone. Therefore, an efficient coupling to external radiation is expected only for sufficiently high values of the wave vector component parallel to the slab surface. This situation is represented in Fig. 6, where the calculated defect mode dispersion for the W1.0 waveguide is repeated in the first and second Brillouin zones, within an extended zone scheme. The light lines in a Si hemisphere at varying incidence angles are also shown (dotted lines) in the figure. We notice that the $\sigma_{k_z} = +1$ mode is characterized by a relatively smooth dispersion over the whole extended zone, whilst the $\sigma_{k_z} = -1$ mode develops almost parallel to the light line of the effective core layer for sufficiently high k values. As previously discussed, this region of strong dispersion is the most interesting one for application purposes, due to the reduced losses expected for a mode with high group velocity. Then, the use of silicon as ATR material is very convenient because it allows covering (virtually) all the frequency-wave vector range available for guided modes in the extended zone. In particular, we notice that the dispersion of the $\sigma_{k_z} = -1$ mode is fully mapped with ATR measurements at incidence angles ranging from about 35° to 60° .

In Fig. 7 (left and central panels) we show the variable-angle TE-polarized ATR spectra of samples W1.0, W1.2, and W1.5, measured at two different values of the azimuthal angle ϕ .³³ All the curves are characterized by relatively sharp features arising from excitation of the defect and bulk modes lying mostly below the light-line (guided modes), which dis-

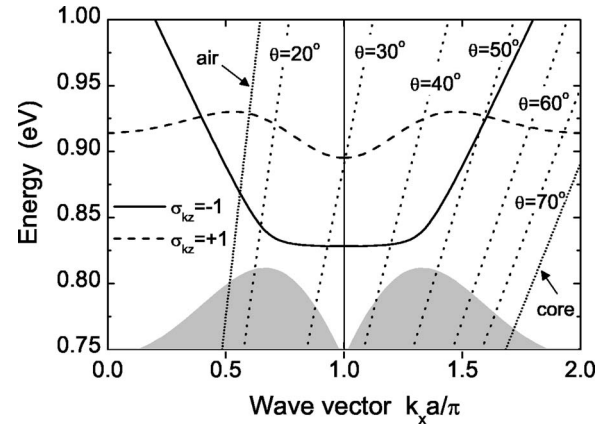


FIG. 6. Calculated dispersion of the two defect modes ($\sigma_{k_z} = \pm 1$) for the W1.0 waveguide with nominal parameters $a = 0.4 \mu\text{m}$, $d = 0.23 \mu\text{m}$, and $r/a = 0.32$, repeated in the first and in the second Brillouin zones. The dispersion of the light lines in a Si hemisphere at different angles of incidence θ are shown as dotted lines. The light lines in air and in the Si core layer (short dots) are indicated by arrows.

play a marked dispersion as a function of the incidence angle. According to symmetry considerations (see Fig. 3), since the coupled components E_y , H_z of the incoming beam have a symmetric profile with respect to the plane of incidence, when this plane is oriented along the line defects (i.e., for $\phi = 0^\circ$) only modes with symmetry $\sigma_{k_z} = -1$ should be observable in the spectra. On the other hand, for $\phi \neq 0^\circ$ the mirror reflection with respect to the incidence plane is no longer a good symmetry operation, and both $\sigma_{k_z} = -1$ and $\sigma_{k_z} = +1$ modes should appear in TE-polarized ATR spectra.

The selection rule that determines the excitation of guided modes is indeed fulfilled in the experiment. In particular, for $\phi = 0^\circ$ (left panels) all the samples display a strong and weakly dispersive resonance around 0.81 eV, together with a weaker but strongly dispersive feature at higher energies. While the former has to be attributed to the lower-edge state of the band-gap opening in the Γ - K direction, the latter corresponds to the excitation of the $\sigma_{k_z} = -1$ defect mode inside the gap. Notice that the higher intensity of resonances corresponding to bulk modes with respect to those of the defect modes follows from measuring a single line defect that is surrounded by many periods of bulk photonic crystal. A higher signal is detected for the bulk modes of the periodic 2D structure, against a weaker signal coming from the single line defect. The linewidth associated to the ATR resonances will be discussed later in this section.

The ATR spectra measured for $\phi = 15^\circ$ show up additional features with respect to the $\phi = 0^\circ$ case, corresponding to the excitation of both odd ($\sigma_{k_z} = -1$) and even ($\sigma_{k_z} = +1$) modes, respectively. Notice also that the strong resonance corresponding to the band-edge photonic mode is now redshifted (not shown in the figure) due to the fact that for $\phi = 15^\circ$ we are no longer aligned to a high symmetry direction of the Brillouin zone. Therefore, even though the measurements at $\phi = 15^\circ$ yield the dispersion of modes of both parities at a glance, the measurements at $\phi = 0^\circ$ are necessary in order to properly evaluate the photonic band edge along Γ - K .

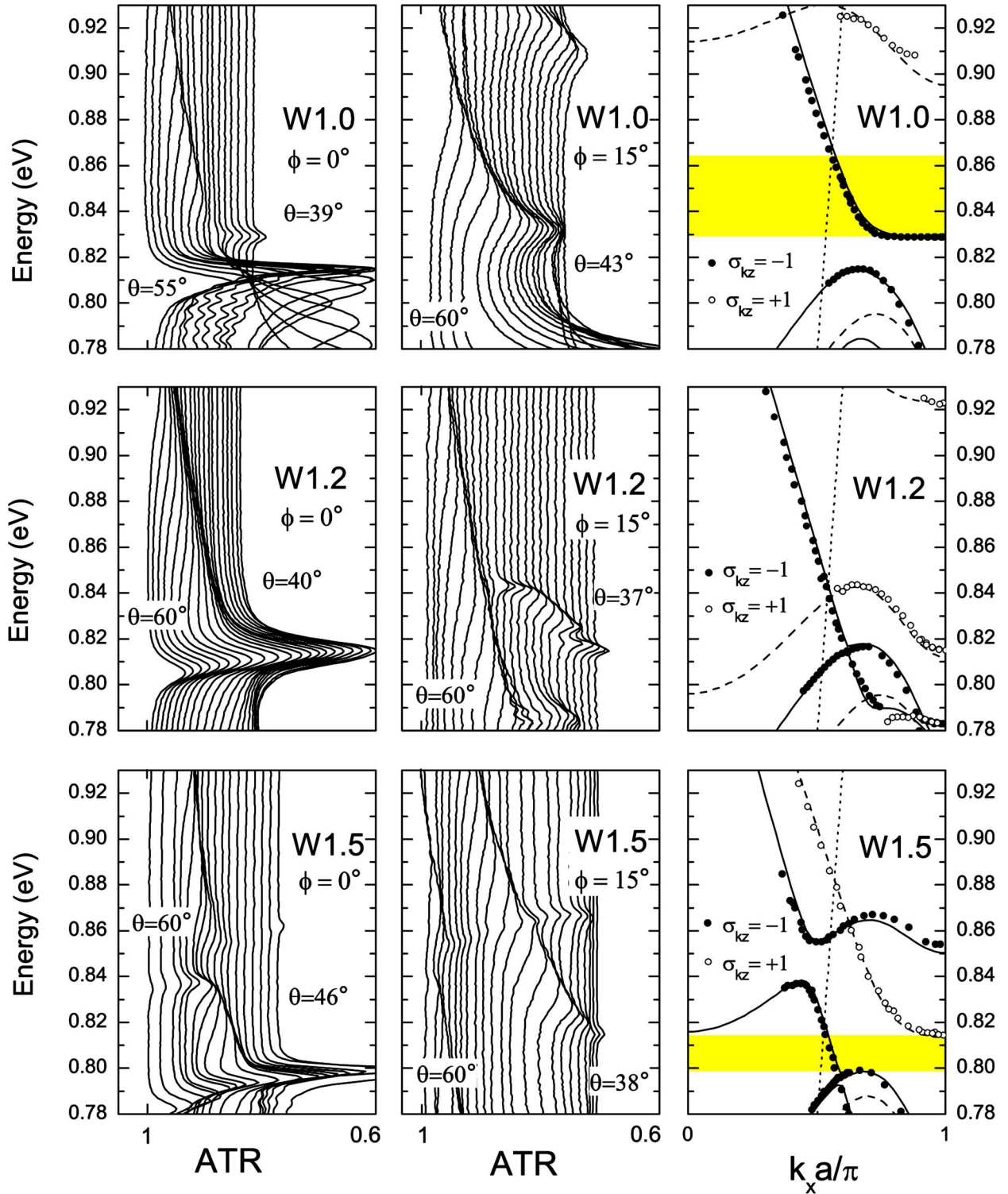


FIG. 7. (Color online) Left and central panels: experimental angle-resolved ATR spectra for samples W1.0, W1.2, and W1.5 measured at two different azimuthal angles $\phi=0^\circ$ and $\phi=15^\circ$, respectively. The curves are slightly shifted horizontally for clarity (Ref. 33). Right panels: measured dispersion of $\sigma_{k_z}=-1$ (closed circles) and $\sigma_{k_z}=+1$ (open circles) photonic modes as derived from ATR spectra, compared to calculated dispersion (solid and dashed lines). The single-mode energy window is highlighted for the W1.0 and W1.5 waveguides.

Notice that, by symmetry considerations, the same information on the $\sigma_{k_z}=+1$ modes could in principle be obtained by performing TM-polarized ATR measurements with $\phi=0^\circ$. However in this case the coupled component is E_x ,

whose field profile along the y direction is oscillating with several nodes as shown in Fig. 3, thereby yielding a very weak coupling with the incoming beam. Moreover, the experimental configuration with TE polarization and tilted

sample results to be more convenient, since it yields the dispersion of guided modes of both parities simultaneously. This allows to immediately recognize the single-mode spectral region.

A comparison between the dispersion of the defect modes as derived from ATR spectra and the calculated band structure for the different samples is presented in Fig. 7, right panels. Here the energies of the resonances observed for both experimental conditions with $\phi=0^\circ$ and $\phi=15^\circ$ at various incidence angles are plotted versus the corresponding wave vector component along the Γ - K direction. The correct wavevector component parallel to the sample surface for $\phi=15^\circ$ is obtained simply by taking $k_{\parallel}=(n\omega/c)\sin\theta\cos\phi$. For all samples we find a very good agreement between the measured and calculated dispersion of the bulk modes and defect modes of both parities. Notice that the only adjustable parameter in the calculation is the hole radius r/a , which is found to be slightly different from the nominal one. The best-fit to experimental data is obtained by setting $r/a=0.335$ for samples W1.0 and W1.2, and $r/a=0.322$ for sample W1.5. Moreover, in order to precisely fit experimental data, the calculations assume nearby holes surrounding the linear defect to have a smaller radius (with a reduction up to 10% with respect to the holes of the perfect lattice). This result is in agreement with the observed reduction of the nearby holes' diameter due to the lower electron dose received during the lithography process.

We notice that in the present ATR measurements the mode dispersion both below and above the air light line is measured. Making reference to Fig. 6, the portion of the defect-mode dispersion that lies above the light line when folded in the first Brillouin zone is probed by ATR measurements at a large angle of incidence, in which the incident beam couples to the dominant mode component lying in the second Brillouin zone. Thus the ATR technique with the use of a Silicon hemisphere enables to map the dispersion of both quasi-guided and truly-guided defect modes at the same time.

We can now trace the evolution in the dispersion properties of the defect modes on increasing the channel width, and

validate the theoretical predictions presented in Sec. II. For the sample W1.0 we find the well known behavior^{7,16,21} with a single-mode region for the $\sigma_{k_z}=-1$ defect mode below the light line. In our sample this single-mode propagation occurs between 0.825 eV and 0.865 eV, as shown in Fig. 7. We notice that previous transmission measurements were able to map the dispersion of the $\sigma_{k_z}=-1$ defect mode,²¹ but the $\sigma_{k_z}=+1$ defect mode was not accessible to the measurements due to its much higher propagation losses. We also notice the very large group velocity dispersion associated with the W1.0 waveguide, in which the defect mode exhibits high group velocity values just below the light line and vanishingly small ones on approaching the Brillouin zone edge. Upon increasing the channel width, the $\sigma_{k_z}=-1$ mode gradually shifts to lower energies and merges with the lower band-gap edge. Simultaneously, an even more pronounced redshift is also observed for the $\sigma_{k_z}=+1$ mode. This causes the single-mode window experienced by the $\sigma_{k_z}=-1$ mode to progressively close and completely disappear for the sample W1.2, as shown in Fig. 7. However, with a further increase of the channel width the $\sigma_{k_z}=+1$ mode completely merges with the continuum of states outside the photonic gap, and a new single-mode window opens up for the $\sigma_{k_z}=-1$ mode around 0.8 eV. As shown in Fig. 7, for sample W1.5 this new single-mode region extends over 18 meV, between 0.8 and 0.818 eV, and it is characterized by a strong dispersion that is very close to the Si light line, giving rise to a high group velocity. Due to the lower losses associated to guided modes with high group velocities, this result may be of considerable interest in the realization of linear PhC waveguides with ultralow losses and single-mode behavior. We stress here that the ability of the ATR technique to probe the dispersion of guided defect modes of both parities with respect to a vertical plane bisecting the waveguide channel is of fundamental importance for the experimental verification that a given structure actually satisfies single-mode requirements.

It is important to discuss the origin of the linewidths of the waveguide modes in the ATR measurements of Fig. 7. To this purpose, in Fig. 8(a) we show a blowup of selected

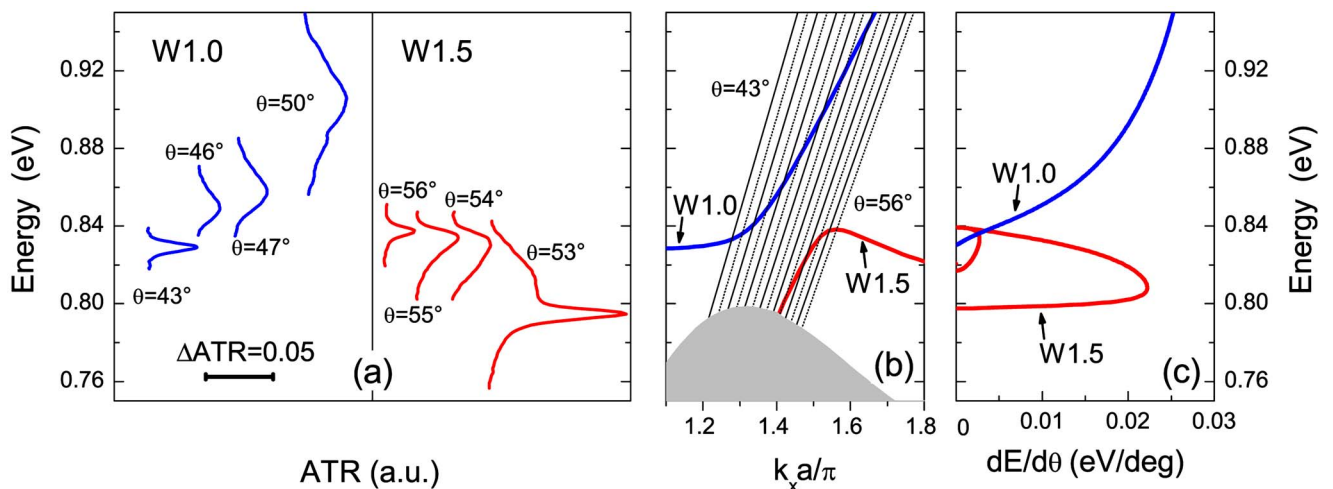


FIG. 8. (Color online) (a) Selected ATR spectra of the W1.0 and W1.5 waveguides for an azimuthal angle $\phi=0^\circ$, (b) corresponding dispersion of the $\sigma_{k_z}=-1$ defect modes in the second Brillouin zone and light lines in the silicon prism at an angular separation $\Delta\theta=1^\circ$ (the gray area denotes the bulk continuum), and (c) derivative of the energy dispersion with respect to the incidence angle.

defect-mode resonances in ATR spectra, referring to the W1.0 and W1.5 waveguides for an azimuthal angle $\phi=0^\circ$, compared to the corresponding dispersions in Fig. 8(b). (In the $\theta=53^\circ$ spectrum the defect mode overlaps the strong bulk resonance at the band edge, which is also shown for comparison.) The spectra of Fig. 8(a), which have a pronounced variation as a function of incidence angle, rule out any possible role of propagation losses in determining the ATR linewidths. Indeed propagation losses are known to be minimum in the region of high group velocity and to increase rapidly in the flat dispersion region of low group velocity.^{10,15,17,20} thus they should follow an opposite trend as compared to what is shown in Fig. 8(a). The origin of the ATR linewidths of defect modes lies in the angular spread of the incident beam, as well as in the prism-induced coupling of guided modes to the radiative region. The first effect can be appreciated by looking at the intersection between the defect-mode dispersion and the light lines at different angles of incidence, shown in Fig. 8(b). Notice that the dispersion is plotted in the second Brillouin zone, i.e., in region of the k - ω plane where the defect modes are more evident in ATR spectra (see Fig. 6 and related discussion). The light lines are plotted at an angular separation of 1° , which corresponds to the estimated resolution of $\pm 0.5^\circ$. When the defect mode dispersion is nearly flat, the energy of the intersection depends weakly on the incidence angle and the linewidth is small (e.g., spectra corresponding $\theta=43^\circ$ and $\theta=56^\circ$ for W1.0 and W1.5, respectively). However, when the defect-mode dispersion is steep with a high group velocity, the intersection point is a very sensitive function of the incidence angle, leading to a much larger linewidth. In Fig. 8(c) we show the derivative of the defect-mode dispersion with respect to the incidence angle: if the angular resolution is $\pm 0.5^\circ$ ($\Delta\theta=1^\circ$), the derivative $dE/d\theta$ is also a measure of the expected energy broadening in eV. The linewidths (in eV/degree) of both W1.0 and W1.5 defect modes are shown in Fig. 8(c) to have a strong energy dependence and to reach values higher than 25 meV for a 1° angular spread. It is interesting to notice that the experimentally observed behavior of the ATR linewidths in Fig. 8(a) follows the same trend as predicted by the function $dE/d\theta$. Furthermore, the asymmetric lineshape observed for the W1.5 defect mode at $\theta=54^\circ$ can be associated to different linewidths in the high- and low-energy regions of the intersection point between the light line and the defect-mode dispersion [see Fig. 8(b)]. This comparison shows that even a small angular spread of the incoming beam may produce a sizeable linewidth enlargement, especially when the light lines in the Silicon prism are nearly parallel to the defect-mode dispersion in the Si PhC waveguides measured in the second Brillouin zone. The small residual linewidths observed for $\theta=43^\circ$ and $\theta=56^\circ$ are related to prism-induced coupling to radiative modes, as already observed and calculated in our previous work.¹⁹ We do not pursue a more quantitative analysis of the ATR linewidths, since this would require a precise knowledge of the incoming beam profile, as well as of the prism-sample separation at all incidence angles. Nevertheless, we emphasize that the linewidths observed in ATR spectra are unrelated to propagation losses, and they are an artifact of the present experimental observation technique. Hence, they do not

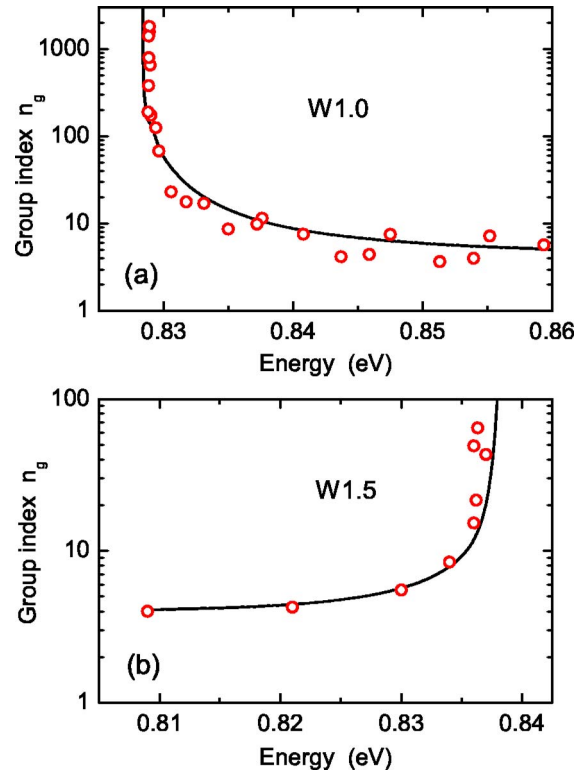


FIG. 9. (Color online) Group index of the $\sigma_{k_z}=-1$ guided modes extracted from experimental dispersion (open circles) and derived from theoretical calculations (continuous lines) for (a) W1.0 and (b) W1.5 waveguides.

jeopardize our conclusions about the presence of a single-mode propagation region in both W1.0 and W1.5 waveguides.

The ATR measurement of the photonic mode dispersion allows determining the group velocity from the derivative $v_g=d\omega/dk$. The group index $n_g=c/v_g$ is displayed in Fig. 9 for the $\sigma_{k_z}=-1$ defect modes of the W1.0 and W1.5 waveguides. The theoretical predictions are also shown for comparison. In the region where the defect modes are strongly dispersive, the group index approaches that of silicon, as expected. On the other hand, in the region where the defect-mode dispersion is flat, the group velocity is strongly reduced and the group index is increased. The effect is particularly prominent for the W1.0 waveguide, where the group index reaches values of the order of 2000. Recently there has been strong interest for slow-light phenomena in photonic crystals structures,^{11,21,34,35} especially in linear waveguides in which propagation losses are very small. The present very high values for the group index can be measured thanks to the experimental technique, which allows determining the defect-mode energy at a specified value of the wave vector. Thus the present ATR experiments prove to be very useful for a precise determination of slowing down of light in linear PhC devices.

IV. CONCLUSIONS

We performed a systematic study of defect-mode dispersion in Silicon photonic crystal waveguides with increased

channel widths. Angle-resolved ATR from the sample surface has been successfully employed for the excitation of truly guided modes by means of a silicon hemisphere, yielding the photonic band dispersion below the light line in a very wide frequency–wave-vector range. The high sensitivity of the technique allows the measurement of membrane-type waveguides containing a single line-defect, thereby yielding the dispersion of defect modes with both parities with respect to a vertical plane bisecting the waveguide channel. This is crucial in order to distinguish the regions of single-mode and multimode propagation.

Results for membranes containing line-defects with various channel widths with respect to the standard W1.0 configuration (one missing row of holes along the Γ - K direction) confirm our theoretical predictions that a convenient single-mode frequency window below the light line exists also for increased-width membrane waveguides. In particular, we observe that as the channel width is increased from $w=1.0w_0$ to $w=1.5w_0$ a single-mode window first closes, then opens up again. The W1.5 waveguide is the optimum situation in

which an increased-width line defect sustains a single truly guided mode with a high group velocity. The group index associated with the defect modes is experimentally determined and reaches values up to 2000 for the flat dispersion region of the W1.0 waveguide. The results are in very good agreement with the theoretical calculations and should be important for the realization of linear photonic crystal waveguides with single-mode behavior and ultralow losses.

ACKNOWLEDGMENTS

The authors are grateful to M. Agio for participation in the early stages of this work and for a critical reading of the manuscript. This research was supported by Ministero dell'Istruzione, dell'Università e della Ricerca (MIUR) through Cofin and FIRB programs and by Fondazione Banca del Monte di Lombardia. Part of the work has been carried out within the European Network of Excellence IST-2-511616-NOE (PHOREMOST).

*Present address: LPN-CNRS, 91460 Marcoussis, France.

- ¹J. D. Joannopoulos, R. D. Meade, and J. N. Winn, *Photonic Crystals: Molding the Flow of Light* (Princeton University Press, Princeton, NJ, 1995).
- ²K. Sakoda, *Optical Properties of Photonic Crystals* (Springer, Berlin, 2001).
- ³S. G. Johnson and J. D. Joannopoulos, *Photonic Crystals: The Road from Theory to Practice* (Kluwer, Dordrecht, 2002).
- ⁴P. St., J. Russell, D. M. Atkin, T. A. Birks, and P. J. Roberts, in *Microcavities and Photonic Band Gaps: Physics and Applications*, Vol. 324 of NATO Advanced Study Institute, Series E: Applied Sciences, edited by J. Rarity and C. Weisbuch (Kluwer Academic Publishers, Dordrecht, The Netherlands, 1996), p. 203.
- ⁵T. F. Krauss, R. M. De La Rue, and S. Brand, *Nature* (London) **383**, 699 (1996).
- ⁶S. G. Johnson, S. Fan, P. R. Villeneuve, J. D. Joannopoulos, and L. A. Kolodziejski, *Phys. Rev. B* **60**, 5751 (1999).
- ⁷A. Chutinan and S. Noda, *Phys. Rev. B* **62**, 4488 (2000).
- ⁸S. G. Johnson, P. R. Villeneuve, S. Fan, and J. D. Joannopoulos, *Phys. Rev. B* **62**, 8212 (2000).
- ⁹T. Baba, A. Motegi, T. Iwai, N. Fukaya, Y. Watanabe, and A. Sakai, *IEEE J. Quantum Electron.* **38**, 743 (2002).
- ¹⁰S. McNab, N. Moll, and Y. Vlasov, *Opt. Express* **11**, 2927 (2003).
- ¹¹M. Notomi, A. Shinya, S. Mitsugi, E. Kuramochi, and H.-Y. Ryu, *Opt. Express* **12**, 1551 (2004).
- ¹²Y. Sugimoto, Y. Tanaka, N. Ikeda, Y. Nakamura, K. Asakawa, and K. Inoue, *Opt. Express* **12**, 1090 (2004).
- ¹³D. Gerace and L. C. Andreani, *Opt. Lett.* **29**, 1897 (2004).
- ¹⁴L. C. Andreani, D. Gerace, and M. Agio, *Photonics Nanostruct. Fundam. Appl.* **2**, 103 (2004).
- ¹⁵D. Gerace and L. C. Andreani, *Opt. Express* **13**, 4939 (2005).
- ¹⁶K. Yamada, H. Morita, A. Shinya, and M. Notomi, *Opt. Commun.* **198**, 395 (2001).

- ¹⁷S. Hughes, L. Ramunno, J. F. Young, and J. E. Sipe, *Phys. Rev. Lett.* **94**, 033903 (2005).
- ¹⁸B. Cluzel, D. Gérard, E. Picard, T. Charvolin, V. Calvo, E. Hadji, and F. de Fornel, *Appl. Phys. Lett.* **85**, 2682 (2004).
- ¹⁹M. Galli, M. Belotti, D. Bajoni, M. Patrini, G. Guizzetti, D. Gerace, M. Agio, L. C. Andreani, and Y. Chen, *Phys. Rev. B* **70**, 081307(R) (2004).
- ²⁰M. Notomi, A. Shinya, K. Yamada, J. Takahashi, C. Takahashi, and Y. Yokohama, *IEEE J. Quantum Electron.* **38**, 736 (2002).
- ²¹M. Notomi, K. Yamada, A. Shinya, J. Takahashi, C. Takahashi, and I. Yokohama, *Phys. Rev. Lett.* **87**, 253902 (2001).
- ²²C. J. M. Smith, H. Benisty, S. Olivier, M. Rattier, C. Weisbuch, T. F. Krauss, R. M. De La Rue, R. Houdré, and U. Oesterle, *Appl. Phys. Lett.* **77**, 2813 (2000).
- ²³S. Olivier, M. Rattier, H. Benisty, C. Weisbuch, C. J. M. Smith, R. M. De La Rue, T. F. Krauss, U. Oesterle, and R. Houdré, *Phys. Rev. B* **63**, 113311 (2001).
- ²⁴H. Benisty, S. Olivier, C. Weisbuch, M. Agio, M. Kafesaki, C. M. Soukoulis, M. Qiu, M. Swillo, A. Karlsson, B. Jaskorzynska, A. Talneau, J. Moosburger, M. Kamp, A. Forchel, R. Ferrini, R. Houdré, and U. Oesterle, *IEEE J. Quantum Electron.* **38**, 770 (2002).
- ²⁵L. C. Andreani and M. Agio, *IEEE J. Quantum Electron.* **38**, 891 (2002).
- ²⁶L. C. Andreani, *Phys. Status Solidi B* **234**, 139 (2002).
- ²⁷L. C. Andreani and M. Agio, *Appl. Phys. Lett.* **82**, 2011 (2003).
- ²⁸D. Gerace and L. C. Andreani, *Phys. Rev. E* **69**, 056603 (2004).
- ²⁹M. Patrini, M. Galli, F. Marabelli, M. Agio, L. C. Andreani, D. Peyrade, and Y. Chen, *IEEE J. Quantum Electron.* **38**, 885 (2002).
- ³⁰D. Peyrade, Y. Chen, A. Talneau, M. Patrini, M. Galli, F. Marabelli, M. Agio, L. C. Andreani, E. Silberstein, and P. Lalanne, *Microelectron. Eng.* **61-62**, 529 (2002).
- ³¹T. Fujita, Y. Sato, T. Kuitani, and T. Ishihara, *Phys. Rev. B* **57**, 12428 (1998).

- ³²V. N. Astratov, D. M. Whittaker, I. S. Culshaw, R. M. Stevenson, M. S. Skolnick, T. F. Krauss, and R. M. De La Rue, *Phys. Rev. B* **60**, R16255 (1999).
- ³³The incidence angles of the ATR spectra in Fig. 7 have been chosen in order to better appreciate the dispersion of the defect modes, and are not always equally spaced. The values of the incidence angles in degrees are specified as follows. For the W1.0 waveguide, $\phi=0$: $\theta=39, 40, 41, 42, 43, 44, 44.5, 45, 45.5, 46, 47, 48, 49, 50, 51, 53, 55$ (17 values). W1.0 waveguide, $\phi=15$: $\theta=43-60, \Delta\theta=1$ (18 values). For the W1.2 waveguide, $\phi=0$: $\theta=40-60, \Delta\theta=1$ (21 values). W1.2 waveguide, $\phi=15$: $\theta=37-60, \Delta\theta=1$ (24 values). For the W1.5 waveguide, $\phi=0$: $\theta=46, 48, 50, 50.5, 51, 51.5, 52, 52.5, 53, 53.5, 54, 54.5, 55, 56, 57, 58, 59, 60$ (18 values). W1.5 waveguide, $\phi=15$: $\theta=38-60, \Delta\theta=1$ (23 values).
- ³⁴H. Gersen, T. J. Karle, R. J. P. Engelen, W. Bogaerts, J. P. Kort-erik, N. F. van Hulst, T. F. Krauss, and L. Kuipers, *Phys. Rev. Lett.* **94**, 073903 (2005).
- ³⁵H. Altug and J. Vučković, *Appl. Phys. Lett.* **86**, 111102 (2005).